Commun. Comput. Phys.
doi: 10.4208/cicp.290112.030812a

Vol. **14**, No. 1, pp. 242-264
July 2013

A Direct Solver for Initial Value Problems of Rarefied Gas Flows of Arbitrary Statistics

Jaw-Yen Yang[1,*], Bagus Putra Muljadi[1,2], Zhi-Hui Li[3,4] and Han-Xin Zhang[3,4]

[1] *Institute of Applied Mechanics, National Taiwan University,Taipei 10764, Taiwan.*
[2] *FCS STAE, Université Paul Sabatier, Institut de mathématiques de Toulouse, Toulouse 31400, France.*
[3] *National Laboratory for Computational Fluid Dynamics, Beijing 100191, China.*
[4] *China Aerodynamics Research and Development Center, Mianyang, 621000, China.*

Received 29 January 2012; Accepted (in revised version) 3 August 2012

Available online 15 November 2012

Abstract. An accurate and direct algorithm for solving the semiclassical Boltzmann equation with relaxation time approximation in phase space is presented for parallel treatment of rarefied gas flows of particles of three statistics. The discrete ordinate method is first applied to discretize the velocity space of the distribution function to render a set of scalar conservation laws with source term. The high order weighted essentially non-oscillatory scheme is then implemented to capture the time evolution of the discretized velocity distribution function in physical space and time. The method is developed for two space dimensions and implemented on gas particles that obey the Maxwell-Boltzmann, Bose-Einstein and Fermi-Dirac statistics. Computational examples in one- and two-dimensional initial value problems of rarefied gas flows are presented and the results indicating good resolution of the main flow features can be achieved. Flows of wide range of relaxation times and Knudsen numbers covering different flow regimes are computed to validate the robustness of the method. The recovery of quantum statistics to the classical limit is also tested for small fugacity values.

AMS subject classifications: 82-08, 82B30, 82B40, 35Q20

Key words: Semiclassical Boltzmann-BGK equation, weighted essentially non-oscillatory, discrete ordinate method.

1 Introduction

In kinetic theory of gases, the Boltzmann equation has been widely used to describe various transport phenomena in classical rarefied gas covering wide range of flow param-

*Corresponding author. *Email addresses:* yangjy@iam.ntu.edu.tw (J.-Y. Yang), muljadi.bp@gmail.com (B. P. Muljadi), zhli0097@x263.net (Z.-H. Li), hanxinzhang@tom.com (H.-X. Zhang)

eters such as Reynolds number, Mach number and Knudsen number. The Chapman-Enskog expansion method is usually applied to the Boltzmann equation to derive closed set hydrodynamic transport equations that apply to a broad range of flow regimes, see [8]. In analogy to the classical Boltzmann equation, a semiclassical Boltzmann equation, which generalizes the collision term in order to treat the collision of particles of quantum statistics, has been developed; For detail, readers may refer to [21, 34]. Hydrodynamic behaviour of quantum gases has been the subject of some prominent researches, see [3, 28, 36], and the application of quantum Boltzmann hydrodynamic equations have been implemented in the analysis of electron flows in quantum semiconductor devices, such as in the works of [2, 12, 37]. In recent years, due to the rapid advancements of microtechnology and nanotechnology, the device or structure characteristic length scales become comparable to the mean free path and the wavelength of energy and information carriers (mainly electrons, photons, phonons, and molecules), some of the classical continuum transport laws are no longer applicable. It is generally believed that the microscopic description of Boltzmann equation (classical and semiclassical) is adequate to treat transport phenomena in the mesoscale range. Different types of carriers may involve simultaneously in a single problem, therefore, it is desirable to have a method that can allow one to treat them in a unified and parallel manner. Indeed, this is the view advocated in micro- and nano-scale energy transport by Chen [9]. With the semiclassical Boltzmann equation, it is possible to describe adequately the mesoscale transport of particles of arbitrary statistics.

The principal difficulty encountered in solving semiclassical Boltzmann equation as derived by Uehling and Uhlenbeck is the same as that encountered in the classical counterpart and is mainly due to the complicated integral nature of its collision term. The relaxation time approximation proposed by Bhatnagar, Gross and Krook (BGK) [4] for the classical Boltzmann equation provides a much simpler form of collision term and retains the principal effects of particle collisions and enables more tractable solution methods. The BGK relaxation time concept is rather general and can be applicable to the semiclassical Boltzmann equation as well. The only change is that the equilibrium Maxwell-Boltzmann distribution in the classical case is replaced by the Bose-Einstein or Fermi-Dirac distribution depending on the types of carrier particles. The semiclassical Boltzmann-BGK equation has been widely applied for electron carrier transport in semiconductor [5–7, 11, 25–27, 29, 30] and phonon energy transport in thermoelectric materials [9]. Similarly, the solution methodology developed for classical Boltzmann-BGK equation can be applied to the semiclassical Boltzmann-BGK equation in phase space. In this work, we aim at developing an accurate direct solver for the semiclassical Boltzmann-BGK equation in phase space that can treat particles of three statistics on equal foot and in a parallel manner. Such a method will allow one to examine the same physical flow problems but with different gas of particles. It is noted that even when solving the problems for the classical Maxwell-Boltzmann statistics, the present formulation allows the analysis fugacity which has not been included in the original Boltzmann-BGK equation [4] nor in most of other existing works based on it. First, depending on

the carrier particles, the discrete ordinate method is used to discretize the velocity (or momentum or wave number) space in the semiclassical Boltzmann-BGK equation into a set of equations for the discrete distribution functions which are continuous in physical space with source terms [40]. Second, the resulting equations can be treated as scalar hyperbolic conservation law with stiff source term whose evolution in space and time can be modeled by existing shock-capturing schemes such as total variation diminishing (TVD) schemes [13] and weighted essentially non-oscillatory (WENO) schemes [38]. The latter is adopted in this paper to describe the evolution of these equations. We develop the method in two space dimensions and validate the method using flow problems of one and two space dimensions. Three main aspects of the developed method are examined and emphasized, namely, the range of relaxation time, the range of Knudsen numbers and the recovery of the classical limit. After the success of these tests, the present method can provide a viable robust tool for treating many modern mesoscale carrier transport phenomena covering electrons and phonons in addition to the usual classical gas molecules. In the area of classical gas flows, the implementation of discrete ordinate method to nonlinear model Boltzmann equations has been developed by Yang and Huang [40] for the rarefied flow computations and has been able to cover broad range of flow regimes. Similar approaches using different high resolution spatial schemes were also given [23, 24]. In this work, the main purposes are first to explore the wide range of physical parameters of the semiclassical Boltzmann-BGK equation and second to examine the effects of particle statistics under the same flow problems. We adopt well established and previously developed spatial high resolution schemes such as TVD [14], NND [42], WENO [17]and compacted WENO [10] methods. Also to exclude the complexity due to solid boundary, we confine here to initial value problems. Under the same motivation as in classical case, the present work is built using discrete ordinate method to describe the hydrodynamic properties of rarefied gases of all the three statistics.

Elements of semiclassical Boltzmann-BGK equation is briefly described in Section 2. Its correlation with hydrodynamic equations is outlined. In Section 3, we describe the use of discrete ordinate method to discretize the particle distribution function into a set of hyperbolic conservation laws with source terms. In the next section, we present the description of fifth-order WENO scheme implementation in capturing the evolution of discretized distribution function equations. In Section 5, numerical experiments of one dimensional semiclassical gas dynamical flows in a shock tube in addition to two dimensional Riemann problems are presented to illustrate the present algorithm. Finally, concluding remarks will be given in Section 6.

2 Semiclassical Boltzmann-BGK equation

In this section, we delineate the elements of semiclassical Boltzmann-BGK equation which we expect to tackle in the present work. Following the works of [21, 34], we consider the extension of the Boltzmann equation to quantum systems due to Uehling and Uhlenbeck

in which they took the Pauli exclusion principle into account.

$$\left(\frac{\partial f}{\partial t}+\frac{\mathbf{p}}{m}\cdot\nabla_x-\nabla U(\mathbf{x},t)\cdot\nabla_{\mathbf{p}}\right)f(\mathbf{p},\mathbf{x},t)=\left(\frac{\delta f}{\delta t}\right)_{coll.}, \tag{2.1}$$

where m is the particle mass, U is the mean field potential and $f(\vec{p},\vec{x},t)$ is the distribution function which represents the average density of particles with momentum $\vec{p}$ at the space-time point $\vec{x},t$. The $(\delta f/\delta t)_{coll.}$ denotes the collision term and according to Uehling and Uhlenbeck [34], it takes the form,

$$\begin{aligned}\left(\frac{\delta f}{\delta t}\right)_{coll.}^{UU}=\int d\mathbf{p}\int d\Omega K(\mathbf{p},\mathbf{q},\Omega)\Big\{&[1+\theta f(\mathbf{p},t)][1+\theta f(\mathbf{q})]f(\mathbf{p}^*,t)f(\mathbf{q}^*,t)\\&-[1+\theta f(\mathbf{p}^*,t)][1+\theta f(\mathbf{q}^*)]f(\mathbf{p},t)f(\mathbf{q},t)\Big\},\end{aligned} \tag{2.2}$$

where $K(\mathbf{p},\mathbf{q},\Omega)$ denotes the collision kernel and Ω is the solid angle and θ is a parameter which specifies the type of particle statistics. Here, for $\theta=+1$, Bose-Einstein particles are considered, for $\theta=-1$, Fermi-Dirac particles, and for $\theta=0$, the Maxwell-Boltzmann classical particles are considered. According to the Boltzmann's H-theorem and conservation conditions, the collision integral of the semiclassical Boltzmann equation will automatically vanish when the distribution functions are in equilibrium and the equilibrium distribution function for general statistics can be expressed as

$$f^{eq}(\mathbf{p},\mathbf{x},t)=\frac{1}{z^{-1}\exp\Big\{\left[\mathbf{p}-m\,\mathbf{u}(\mathbf{x},t)\right]^2/2mk_BT(\mathbf{x},t)\Big\}-\theta}, \tag{2.3}$$

where $\mathbf{u}(\mathbf{x},t)$ is the mean velocity, $T(\mathbf{x},t)$ is temperature, k_B is the Boltzmann constant and $z(\mathbf{x},t)=exp(\mu(\mathbf{x},t)/k_BT(\mathbf{x},t))$ is the fugacity, where μ is the chemical potential. In (2.3), $\theta=-1$ denotes the Fermi-Dirac statistics, $\theta=+1$, the Bose-Einstein statistics and $\theta=0$ denotes the Maxwell-Boltzmann statistics. We note that even with the case of $\theta=0$, we still have chemical potential μ or fugacity z which is rather different from the usual classical Maxwellian distribution. To avoid the mathematical difficulty caused by the nonlinear integral collision term, the relaxation time concept of Bhatnagar, Gross and Krook is generally applied to replace the collision term of Uehling and Uhlenbeck, thus the semiclassical Boltzmann-BGK equation reads

$$\left(\frac{\partial f}{\partial t}+\frac{\mathbf{p}}{m}\cdot\nabla_x-\nabla U(\mathbf{x},t)\cdot\nabla_{\mathbf{p}}\right)f(\mathbf{p},\mathbf{x},t)=\left(\frac{\delta f}{\delta t}\right)_{coll.}^{BGK}=-\frac{f-f^{eq}}{\tau}. \tag{2.4}$$

Here, τ is the relaxation time and needs to be specified for each carrier scattering.

The macroscopic dynamic variables of interest such as number density, momentum density and energy density are low order moments of the distribution function and are

defined by:

$$n(\mathbf{x},t)=\int \frac{d\mathbf{p}}{h^3} f(\mathbf{p},\mathbf{x},t), \tag{2.5a}$$

$$\mathbf{j}(\mathbf{x},t)=\int \frac{d\mathbf{p}}{h^3}\frac{\mathbf{p}}{m} f(\mathbf{p},\mathbf{x},t)=n(\mathbf{x},t)\mathbf{u}(\mathbf{x},t), \tag{2.5b}$$

$$\epsilon(\mathbf{x},t)=\int \frac{d\mathbf{p}}{h^3}\frac{\mathbf{p}^2}{2m} f(\mathbf{p},\mathbf{x},t), \tag{2.5c}$$

where h is Planck's constant. Other higher-order moments such as stress tensor P_{ij} and the heat flux vector $\Phi_i(\mathbf{x},t)$ can also be defined accordingly as

$$P_{ij}(\mathbf{x},t)=\int \frac{d\mathbf{p}}{h^3}\left(\frac{p_i}{m}-u_i\right)\left(\frac{p_j}{m}-u_j\right) f(\mathbf{p},\mathbf{x},t), \tag{2.6a}$$

$$\Phi_i(\mathbf{x},t)=\int \frac{d\mathbf{p}}{h^3}\frac{(\mathbf{p}-m\mathbf{u})^2}{2m}\left(\frac{p_i}{m}-u_i\right) f(\mathbf{p},\mathbf{x},t). \tag{2.6b}$$

The conservation laws of macroscopic properties can be obtained by multiplying Eq. (2.1) respectively by 1, $\mathbf{p}$ and $\mathbf{p}^2/2m$ and integrating the resulting equations over all $\mathbf{p}$. Consequently, the integrals of the collision terms in all three cases vanish automatically resulting in the conservation laws in the form of differential equations for the conserved macroscopic quantities i.e., number density $n(\mathbf{x},t)$, momentum density $mn\mathbf{u}(\mathbf{x},t)$, and energy density $\epsilon(\mathbf{x},t)$ as follow:

$$\frac{\partial n(\mathbf{x},t)}{\partial t}+\nabla_x\cdot\mathbf{j}(\mathbf{x},t)=0, \tag{2.7a}$$

$$\frac{\partial m\mathbf{j}(\mathbf{x},t)}{\partial t}+\nabla_x\cdot\int \frac{d\mathbf{p}}{h^3}\mathbf{p}\frac{\mathbf{p}}{m} f(\mathbf{p},\mathbf{x},t)=-n(\mathbf{x},t)\nabla_{\mathbf{x}}U(\mathbf{x},t), \tag{2.7b}$$

$$\frac{\partial \epsilon(\mathbf{x},t)}{\partial t}+\nabla_x\cdot\int \frac{d\mathbf{p}}{h^3}\frac{\mathbf{p}}{m}\frac{\mathbf{p}^2}{2m} f(\mathbf{p},\mathbf{x},t)=-\mathbf{j}(\mathbf{x},t)\cdot\nabla_{\mathbf{x}}U(\mathbf{x},t). \tag{2.7c}$$

Derivations of the semiclassical Euler and Navier-Stokes equations from the Boltzmann-BGK equation can be obtained from the zeroth order and first order solutions via the Chapman and Enskog expansion [8]. Also, the transport coefficients such as the viscosity η and the thermal conductivity κ can be derived in terms of the relaxation time as

$$\eta=\tau n k_B T\frac{\mathcal{Q}_2(z)}{\mathcal{Q}_1(z)}, \tag{2.8a}$$

$$\kappa=\tau\frac{5k_B}{2m}nk_BT\left[\frac{7}{2}\frac{\mathcal{Q}_3(z)}{\mathcal{Q}_1(z)}-\frac{5}{2}\frac{\mathcal{Q}_2(z)}{\mathcal{Q}_1(z)}\right], \tag{2.8b}$$

where $\mathcal{Q}_\nu(z)$ is the Fermi or Bose function of order ν. For similar results derived from the linearized semiclassical Boltzmann equation, see [28]. Here the case of two space

dimensions is assumed. The relaxation times for various scattering mechanisms of different carrier transport in semiconductor devices including electrons, holes, phonons and others have been proposed [15].

In this work, we will also consider the case of *semiclassical Euler* limit in which the particle distribution function is always in equilibrium, i.e., $f=f^{eq}$ and the collision term of Eq. (2.1) vanishes automatically. In the later section, we will present the comparison of our results with those of the semiclassical Euler solutions. In recent years, notable numerical methods to describe the ideal quantum gas flows have been developed, see [32, 39, 41].

2.1 Fermi and Bose functions in relation to hydrodynamics properties

Before we proceed, without losing generality, we neglect the influence of externally applied field $U(\mathbf{x},t)$. To illustrate the present method, we formulate the Fermi - Dirac equilibrium distribution in two spatial dimension as the following.

$$f^{eq}(p_x,p_y,x,y,t)=\frac{1}{z^{-1}\exp((p_x-mu_x)^2+(p_y-mu_y)^2)/(2mk_BT(x,y,t))+1}. \tag{2.9}$$

In a closed form in terms of quantum functions, we replace the distribution function f with f^{eq} which automatically reduces the source term in the BGK Boltzmann equation to zero. The macroscopic moments, i.e., number density $n(x,y,t)$, momentum $j(x,y,t)$ and energy density $\epsilon(x,y,t)$ are given by

$$n(x,y,t)=\int\int\frac{dp_xdp_y}{h^2}f^{eq}(p_x,p_y,x,y,t)=\frac{\mathcal{Q}_1(z)^2}{\lambda}, \tag{2.10a}$$

$$j_x(x,y,t)=\int\int\frac{dp_xdp_y}{h^2}\frac{p_x}{m}f^{eq}(p_x,p_y,x,y,t)=n(x,y,t)u_x(x,y,t), \tag{2.10b}$$

$$j_y(x,y,t)=\int\int\frac{dp_xdp_y}{h^2}\frac{p_y}{m}f^{eq}(p_x,p_y,x,y,t)=n(x,y,t)u_y(x,y,t), \tag{2.10c}$$

$$\begin{aligned}\epsilon(x,y,t)&=\int\int\frac{dp_xdp_y}{h^2}\frac{p_x^2+p_y^2}{2m}f^{eq}(p_x,p_y,x,y,t)\\&=\frac{\mathcal{Q}_2(z)}{\beta\lambda^2}+\frac{1}{2}mn(u_x^2+u_y^2)=\frac{P(x,y,t)}{(\gamma+1)}+\frac{1}{2}mn(u_x^2+u_y^2),\end{aligned} \tag{2.10d}$$

where $\lambda=\sqrt{\frac{\beta h^2}{2\pi m}}$ is the thermal wavelength and $\beta=1/k_BT(x,y,t)$. The functions $\mathcal{Q}_\nu(z)$ of order ν are respectively defined for Fermi-Dirac and Bose-Einstein statistics as

$$\mathcal{F}_\nu(z)\equiv\frac{1}{\Gamma(\nu)}\int_0^\infty dx\frac{x^{\nu-1}}{z^{-1}e^x+1}\approx\sum_{l=1}^\infty(-1)^{l-1}\frac{z^l}{l^\nu}, \tag{2.11a}$$

$$\mathcal{B}_\nu(z)\equiv\frac{1}{\Gamma(\nu)}\int_0^\infty dx\frac{x^{\nu-1}}{z^{-1}e^x-1}\approx\sum_{l=1}^\infty\frac{z^l}{l^\nu}. \tag{2.11b}$$

Here, $\mathcal{F}_\nu(z)$ applies for Fermi-Dirac integral and $\mathcal{B}_\nu(z)$ for Bose-Einstein's, whereas $\Gamma(\nu)$ is gamma function. The definition of macroscopic quantities in terms of Fermi or Bose function applies for both cases of quantum distributions. One only needs to replace Fermi function with Bose function or vice versa whilst maintaining the same procedure.

2.2 Classical limit

Note that for $z \ll 1$, both $\mathcal{Q}_\nu(z)$ functions for all ν behave like z itself, i.e., $\mathcal{Q}_\nu(z) \approx z$. Physically, a large and negative value of chemical potential of a dilute system and high temperature environment do correspond to small z. On the other hand, we know that at the low temperature, the Fermi-Dirac case displays its most distinctive property in terms of one particle per one energy level mapping. We may intuitively say that the hydrodynamic properties of classical case can be acquired by replacing the $\mathcal{Q}_\nu(z)$ function into z itself. Mathematically, we can obtain the classical hydrodynamic properties by applying the same procedure to the Maxwell-Boltzmann statistics as done to the other quantum statistics. For $\theta = 0$, the distribution function becomes

$$f^{MB}(p_x,p_y,x,y,t) = 1/\left\{z^{-1}\exp\left\{\left[(p_x-mu_x)^2+(p_y-mu_y)^2\right]/2mk_BT\right\}\right\}. \tag{2.12}$$

In this case, no approximation for $\mathcal{Q}_\nu(z)$ is required and the macroscopic values for two spatial dimensions can be obtained by

$$n_c(x,y,t) = \int\int \frac{dp_x dp_y}{h^2} f^{MB}(p_x,p_y,x,y,t) = \frac{z}{\lambda^2}. \tag{2.13}$$

In other words, in the classical limit,

$$z(x,y,t) = e^{\mu(x,y,t)/k_BT(x,y,t)} = \lambda^2 n_c(x,y,t), \tag{2.14a}$$

$$\mu(x,y,t) = k_BT(x,y,t)\ln(\lambda^2 n_c(x,y,t)). \tag{2.14b}$$

In the later section, we shall see the numerical examples that compare Fermi and Bose gas to the classical limit.

2.3 Normalization

Before proceeding to discretize the equation, in this section we introduce the characteristic properties of V_∞ and t_∞ for the purpose of normalization. The characteristic velocity and time can be defined as,

$$V_\infty = \sqrt{\frac{2k_BT_\infty}{m}}, \qquad t_\infty = \frac{L}{V_\infty}, \tag{2.15}$$

with L defined as the characteristic length of the problem. Hence the definitions of non-dimensional variables are introduced as

$$(\hat{t},\hat{\tau})=(t,\tau)/t_\infty,\qquad (\hat{u}_x,\hat{v}_x)=(u_x,v_x)/V_\infty,\qquad \hat{x}=x/L,\hat{T}=T/T_\infty, \tag{2.16a}$$

$$(\hat{u}_y,\hat{v}_y)=(u_y,v_y)/V_\infty,\qquad \hat{y}=y/L,\hat{n}=n/\left(\frac{m^2V_\infty^2}{h^2}\right), \tag{2.16b}$$

$$\hat{j}=j/\left(\frac{m^2V_\infty^3}{h^2}\right),\qquad \hat{\epsilon}=\epsilon/\left(\frac{m^3V_\infty^4}{h^2}\right),\qquad \hat{f}=f. \tag{2.16c}$$

Hence the normalized semiclassical Boltzmann-BGK equation,

$$\frac{\partial\hat{f}(\hat{v}_x,\hat{v}_y,\hat{x},\hat{y},\hat{t})}{\partial\hat{t}}+\hat{v}_x\frac{\partial\hat{f}(\hat{v}_x,\hat{v}_y,\hat{x},\hat{y},\hat{t})}{\partial\hat{x}}+\hat{v}_y\frac{\partial\hat{f}(\hat{v}_x,\hat{v}_y,\hat{x},\hat{y},\hat{t})}{\partial\hat{y}}=-\frac{\hat{f}-\hat{f}^{eq}}{\hat{\tau}}, \tag{2.17}$$

with $\hat{v}_x$ and $\hat{v}_y$ as particle velocities. Neglecting the *hat* sign, the normalized two-dimensional semiclassical equilibrium distribution function becomes

$$f^{eq}(v_x,v_y,x,y,t)=\frac{1}{z^{-1}\exp((v_x-u_x)^2+(v_y-u_y)^2)/T-\theta}. \tag{2.18}$$

3 Application of discrete ordinate method

As applied by Huang and Giddens [16] and Shizgal [33] to the linearized Boltzmann-BGK equation, the discrete ordinate method represents functions by a set of discrete points that coincide with the evaluation points in a quadrature rule. The method replaces the original functional dependency on the integral variable by a set of functions with N elements of $W_if(x_i)$ with $i=1,\cdots,N$. The points x_i are quadrature points and W_i are the corresponding weights of the integration rule

$$\int_a^b W(x)f(x)dx=\sum_{i=1}^{N}W_if(x_i). \tag{3.1}$$

The interval $[a,b]$ will be either $[0,\infty]$ or $[-\infty,\infty]$ depending on considered application. Different weighting function $W(x)$ is addressed accordingly. In general, in view of the fact that in the classical limit all three statistics will coincide with each other, we shall employ the Gauss-Hermite quadrature for all three statistics. This method is beneficial given the fact that in the end, we are not just interested in the distribution function itself but also in the macroscopic moments and the evaluations of the macroscopic moments are also done with the same quadrature. The discrete ordinate method has been applied to the classical nonlinear model Boltzmann equations for rarefied flow computations [40]. By applying the discrete ordinate method to Eq. (2.17), the distribution function in phase space $f(v_x,v_y,x,y,t)$ can be rendered into a set of hyperbolic conservation equation with

source terms for $f_{\sigma,\delta}(x,y,t)$ in the physical space, where $\sigma=-N_1,\cdots,-1,1,\cdots,N_1$ and $\delta=-N_2,\cdots,-1,1,\cdots,N_2$. The resulting equations are a set of

$$\frac{\partial f_{\sigma,\delta}(x,y,t)}{\partial t}+v_\sigma\frac{\partial f_{\sigma,\delta}(x,y,t)}{\partial x}+v_\delta\frac{\partial f_{\sigma,\delta}(x,y,t)}{\partial y}=-\frac{f_{\sigma,\delta}-{f_{\sigma,\delta}}^{eq}}{\tau}, \tag{3.2}$$

with $f_{\sigma,\delta}$, v_σ and v_δ represent the values of respectively f, v_x and v_y evaluated at the discrete velocity points σ and δ.

3.1 Quadrature methods

In two-dimensional case, we may apply Gauss-Hermite quadrature rule over the interval $[-\infty,\infty]$. The Gauss-Hermite quadrature rule reads,

$$\int_{-\infty}^{\infty}\int_{-\infty}^{\infty}e^{-{v_x}^2}e^{-{v_y}^2}f(v_x,v_y)dv_xdv_y\approx\sum_{\sigma=-N_1}^{N_1}\sum_{\delta=-N_2}^{N_2}W_\sigma W_\delta f_{\sigma,\delta} \tag{3.3a}$$

or

$$\int_{-\infty}^{\infty}\int_{-\infty}^{\infty}e^{-{v_x}^2}e^{-{v_y}^2}[e^{{v_x}^2}e^{{v_y}^2}f(v_x,v_y)dv_xdv_y]\approx\sum_{\sigma=-N_1}^{N_1}\sum_{\delta=-N_2}^{N_2}W_\sigma W_\delta e^{{v_\sigma}^2}e^{{v_\delta}^2}f_{\sigma,\delta}. \tag{3.3b}$$

The discrete points v_α and weight W_α, with $\alpha=\sigma,\delta$, are tabulated in the table of the Gauss-Hermite quadrature, see [1] and can be found through

$$W_\alpha=\frac{2^{l-1}l!\sqrt{\pi}}{l^2[H_{l-1}(v_\alpha)]^2}, \tag{3.4}$$

with l is number of quadrature points and v_α are the roots of the Hermite polynomial $H_l(v)$ Once the discretized functions $f_{\sigma,\delta}(x,y,t)$ are solved, for every time level we can acquire and update the macroscopic moments in the physical space using a selected quadrature method as described below.

$$\begin{aligned}n(x,y,t)&=\int_{-\infty}^{\infty}\left[f(v_x,v_y,x,y,t)e^{{v_x}^2}e^{{v_y}^2}\right]e^{-{v_x}^2}e^{-{v_y}^2}dv_xdv_y\\&=\sum_{\sigma=-N_1}^{N_1}\sum_{\delta=-N_2}^{N_2}W_\sigma W_\delta e^{{v_\sigma}^2}e^{{v_\delta}^2}f_{\sigma,\delta},\end{aligned} \tag{3.5a}$$

$$\begin{aligned}j_x(x,y,t)&=\int_{-\infty}^{\infty}\left[v_xf(v_x,v_y,x,y,t)e^{{v_x}^2}e^{{v_y}^2}\right]e^{-{v_x}^2}e^{-{v_y}^2}dv_xdv_y\\&=\sum_{\sigma=-N_1}^{N_1}\sum_{\delta=-N_2}^{N_2}v_\sigma W_\sigma W_\delta e^{{v_\sigma}^2}e^{{v_\delta}^2}f_{\sigma,\delta}=n(x,y,t)\,u_x(x,y,t),\end{aligned} \tag{3.5b}$$

$$\begin{aligned}\epsilon(x,y,t)&=\int_{-\infty}^{\infty}\left[\frac{v_x^2+v_y^2}{2}f(v_x,v_y,x,y,t)e^{{v_x}^2}e^{{v_y}^2}\right]e^{-{v_x}^2}e^{-{v_y}^2}dv_xdv_y\\&=\sum_{\sigma=-N_1}^{N_1}\sum_{\delta=-N_2}^{N_2}\left(\frac{v_\sigma^2+v_\delta^2}{2}\right)W_\sigma W_\delta e^{{v_\sigma}^2}e^{{v_\delta}^2}f_{\sigma,\delta}.\end{aligned} \tag{3.5c}$$

Pressure $P(x,y,t)$ can be defined as

$$P(x,y,t)=\left[\epsilon(x,y,t)-\frac{1}{2}n(x,y,t)(u_x^2+u_y^2)\right](\gamma-1). \tag{3.6}$$

The value of relaxation time is given by

$$\tau=\eta/P. \tag{3.7}$$

Here, we note that the basic criteria of choosing different quadratures is to guarantee that the macroscopic moments can be accurately computed which requiring the accurate representation of the distribution function with suitable velocity range being covered. The equally spaced Newton-Cotes formula can also be used if one needs to cover the high energy tail of the distribution function.

4 Numerical method

4.1 Application of weighted essentially non-oscillatory scheme

In this section, we describe the numerical algorithm to solve the set of equations (3.2). A class of WENO schemes is implemented to solve the set of conservation laws with source terms. We firstly discretize the space x,y and time t into a number of cells centered at i,j at time n, hence we approximate $f_{\sigma,\delta}$ by ${f_{\sigma,\delta}}_{i,j}^{n}$. In terms of numerical fluxes, the evolution from n^{th} time level to $(n+1)^{th}$ time level is expressed by

$$\begin{aligned}{f_{\sigma,\delta}}_{i,j}^{n+1}={f_{\sigma,\delta}}_{i,j}^{n}&-\frac{\Delta t}{\Delta x}\left(F^N_{i+1/2,j}-F^N_{i-1/2,j}\right)\\&-\frac{\Delta t}{\Delta y}\left(G^N_{i,j+1/2}-G^N_{i,j-1/2}\right)+\frac{\Delta t}{\tau}\left({f^{eq}_{\sigma,\delta}}_{i,j}^{n}-{f_{\sigma,\delta}}_{i,j}^{n}\right),\end{aligned} \tag{4.1}$$

where the numerical fluxes are defined by

$$F^N_{i+1/2,j}=F^+_{i+1/2,j}+F^-_{i+1/2,j},\qquad G^N_{i,j+1/2}=G^+_{i,j+1/2}+G^-_{i,j+1/2}, \tag{4.2}$$

where the split flux vectors are defined by

$$F^+_{i,j}=v^+_\sigma f_{\sigma,\delta_{i,j}},\qquad F^-_{i,j}=v^-_\sigma f_{\sigma,\delta_{i,j}}, \tag{4.3a}$$

$$G^+_{i,j}=v^+_\delta f_{\sigma,\delta_{i,j}},\qquad G^-_{i,j}=v^-_\delta f_{\sigma,\delta_{i,j}}. \tag{4.3b}$$

Here, $v^\pm_\sigma=(v_\sigma\pm|v_\sigma|)/2$ and $v^\pm_\delta=(v_\delta\pm|v_\delta|)/2$. The time step Δt is chosen to be less than the local relaxation time, τ. In this work, a fifth-order accurate $(r=3)$ WENO (from now

on, this will be denoted as WENO3) scheme is considered for the spatial difference of numerical fluxes with the expression follows below:

$$F^+_{i+1/2,j}=\omega^+_0\left(\frac{2}{6}F^+_{i-2,j}-\frac{7}{6}F^+_{i-1,j}+\frac{11}{6}F^+_{i,j}\right)+\omega^+_1\left(-\frac{1}{6}F^+_{i-1,j}+\frac{5}{6}F^+_{i,j}+\frac{2}{6}F^+_{i+1,j}\right)$$
$$+\omega^+_2\left(\frac{2}{6}F^+_{i,j}+\frac{5}{6}F^+_{i+1,j}-\frac{1}{6}F^+_{i+2,j}\right), \tag{4.4a}$$

$$\omega^+_k=\frac{\alpha^+_k}{\alpha^+_0+\alpha^+_1+\alpha^+_2}, \qquad k=0,1,2, \tag{4.4b}$$

$$\alpha^+_0=\frac{1}{10(\epsilon+IS^+_0)^2}, \qquad \alpha^+_1=\frac{6}{10(\epsilon+IS^+_1)^2}, \qquad \alpha^+_2=\frac{3}{10(\epsilon+IS^+_2)^2}, \tag{4.4c}$$

$$IS^+_0=\frac{13}{12}\left(F^+_{i-2,j}-2F^+_{i-1,j}+F^+_{i,j}\right)^2+\frac{1}{4}\left(F^+_{i-2,j}-4F^+_{i-1,j}+3F^+_{i,j}\right)^2, \tag{4.4d}$$

$$IS^+_1=\frac{13}{12}\left(F^+_{i-1,j}-2F^+_{i,j}+F^+_{i+1,j}\right)^2+\frac{1}{4}\left(F^+_{i-1,j}-F^+_{i+1,j}\right)^2, \tag{4.4e}$$

$$IS^+_2=\frac{13}{12}\left(F^+_{i,j}-2F^+_{i+1,j}+F^+_{i+2,j}\right)^2+\frac{1}{4}\left(3F^+_{i,j}-4F^+_{i+1,j}+F^+_{i+2,j}\right)^2. \tag{4.4f}$$

The numerical flux for the negative part is given by

$$F^-_{i+1/2,j}=\omega^-_0\left(-\frac{1}{6}F^-_{i-1,j}+\frac{5}{6}F^-_{i,j}+\frac{2}{6}F^-_{i+1,j}\right)+\omega^-_1\left(\frac{2}{6}F^-_{i,j}+\frac{5}{6}F^-_{i+1,j}-\frac{1}{6}F^-_{i+2,j}\right)$$
$$+\omega^-_2\left(\frac{11}{6}F^-_{i+1,j}-\frac{7}{6}F^-_{i+2,j}+\frac{2}{6}F^-_{i+3,j}\right), \tag{4.5a}$$

$$\omega^-_k=\frac{\alpha^-_k}{\alpha^-_0+\alpha^-_1+\alpha^-_2}, \qquad k=0,1,2, \tag{4.5b}$$

$$\alpha^-_0=\frac{3}{10(\epsilon+IS^-_0)^2}, \qquad \alpha^-_1=\frac{6}{10(\epsilon+IS^-_1)^2}, \qquad \alpha^-_2=\frac{1}{10(\epsilon+IS^-_2)^2}, \tag{4.5c}$$

$$IS^-_0=\frac{13}{12}\left(F^-_{i-1,j}-2F^-_{i,j}+F^-_{i+1,j}\right)^2+\frac{1}{4}\left(F^-_{i-1,j}-4F^-_{i,j}+3F^-_{i+1,j}\right)^2, \tag{4.5d}$$

$$IS^-_1=\frac{13}{12}\left(F^-_{i,j}-2F^-_{i+1,j}+F^-_{i+2,j}\right)^2+\frac{1}{4}\left(F^-_{i,j}-F^-_{i+2,j}\right)^2, \tag{4.5e}$$

$$IS^-_2=\frac{13}{12}\left(F^-_{i+1,j}-2F^-_{i+2,j}+F^-_{i+3,j}\right)^2+\frac{1}{4}\left(3F^-_{i+1,j}-4F^-_{i+2,j}+F^-_{i+3,j}\right)^2. \tag{4.5f}$$

The expression of $G^+_{i,j+1/2}$ and $G^-_{i,j+1/2}$ can be derived in a similar fashion.

4.2 Application of total variation diminishing (TVD) scheme

For comparison purpose, we also implement a second-order TVD scheme. Under the same expression as Eq. (4.1), we can also define the numerical fluxes for a TVD scheme

given by

$$F^N_{i+1/2,j}=\left(F^+_{i+1/2,j}+F^-_{i+1/2,j}\right)+\frac{1}{2}\left[\mathrm{sgn}(v_\sigma)-|v_\sigma|\right]\left[v^+_\sigma\Delta x\phi(\theta_{xi,j})+v^-_\sigma\Delta x\phi(\theta_{xi+1,j})\right], \tag{4.6}$$

with $\phi(\theta_{xi,j})$ chosen to be the van Leer limiter [35] given by

$$\phi(\theta_{xi,j})=\frac{(|\theta_{xi,j}|+\theta_{xi,j})}{1+|\theta_{xi,j}|}, \tag{4.7a}$$

$$\theta_{xi,j}=\frac{f_{\sigma,\delta^n_{i'+1,j}}-f_{\sigma,\delta^n_{i',j}}}{f_{\sigma,\delta^n_{i+1,j}}-f_{\sigma,\delta^n_{i,j}}},\qquad i'=i-\mathrm{sgn}\left(v_\sigma\frac{\Delta t}{\Delta x}\right). \tag{4.7b}$$

The expression of $G^N_{i,j+1/2}$ can be derived similarly with i' then becomes $i'=i-\mathrm{sgn}\left(v_\delta\frac{\Delta t}{\Delta y}\right)$. Additionally, the comparison between the results generated using WENO3 and those using TVD will also be given in the later section. After acquiring the macroscopic moments, we need to update the values of z and T. To solve $z(x,y,t)$, which is the root of equation

$$\Psi_2(z)=2\epsilon-\frac{\mathcal{Q}_2(z)}{\pi}\left(\frac{n}{\mathcal{Q}_1(z)}\right)^2-n(u_x^2+u_y^2), \tag{4.8}$$

we can use a range of numerical root finding methods. Note that Eq. (4.8) can be derived from Eqs. (2.10a)-(2.10d). In this paper, the bisection method is used to solve z from Eq. (4.8). After z is acquired, we can immediately find T before advancing to the solution of the next time step.

5 Computational results

In this section we present the results of selected computational tests. Here, we test our algorithm to solve one-dimensional shock tube flows and two-dimensional Riemann's problems of semiclassical gas dynamics.

5.1 One-dimensional shock tube problems

In this problem, a diaphragm, which is located at $x=0.5$, separating two regions of gases of arbitrary statistics, each remains in a constant equilibrium state at initial time $t=0$. The macroscopic properties on both sides of the diaphragm are different. Then the diaphragm is removed and flow structures consisting of moving shock wave, contact discontinuity and expansion fan are generated.

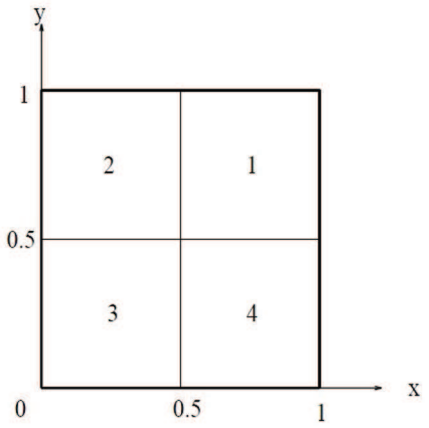

Figure 1: Geometry of the 2-D Riemann's problems set up.

5.1.1 Mesh refinement

As the computational grid mesh is refined, a correct algorithm should give the numerical truncation error decreased. This results in sharper flow profiles especially in regions where rarefaction fans, contact discontinuities and shocks are present. We specified the initial condition for Fermion gas at the left side and right side respectively to be $(n_l,u_l,T_l)=(0.724,0,4.38)$ and $(n_r,u_r,T_r)=(0.589,0,8.97)$ which correspond to $z_l=0.225$ and $z_r=0.12$. In this mesh refinement test, three uniform grid systems are used with $100\,,200$ and 400 cells. The flow is computed with CFL $=0.2$ and Knudsen number $Kn=0.0001$ and the results are output at $t=0.1$. In this example, we define the Knudsen number based on the relation $Kn=\lambda_\infty/L$ which indicates the degree of rarefaction of the gas flow. The characteristic length chosen for this case is the length of the shock tube, i.e., 1. Hence by choosing a specific Knudsen number, we automatically specify the mean free path. Here, the relaxation time will vary with Kn number according to $\tau=\frac{5\sqrt{\pi}Kn}{8nT^{(1-\chi)}}\frac{\mathcal{Q}_1(z)}{\mathcal{Q}_2(z)}$, where $\chi=1$. The quadrature method used in this example is Gauss-Hermite with 20 discrete velocity points and the WENO3 method is used. Fig. 2 shows the grid convergence of density profiles with the main features of shock tube flow, namely, shock wave, contact discontinuity and expansion fan all well captured. We remark that even small Kn=0.0001 is used there still exists some physical viscosity so that the flow profiles are not so sharp as that of the Euler solution. As can be observed from these results, the use of 100 cells for this case is adequate.

5.1.2 Application of varying Knudsen numbers

The initial condition specified here is applied to Fermion gas with the same values as those set in the first and second test cases except for the application of varying Knudsen numbers ranging from 0.1 to 0.0001. The profiles are compared to those acquired in the Euler limit in which $f=f^{(0)}$ so that the source term vanishes automatically. Fig. 3 shows

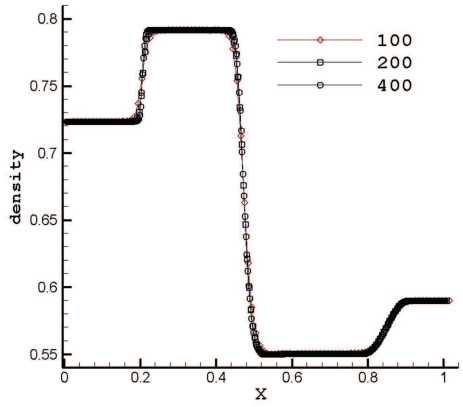

Figure 2: Mesh refinement test.

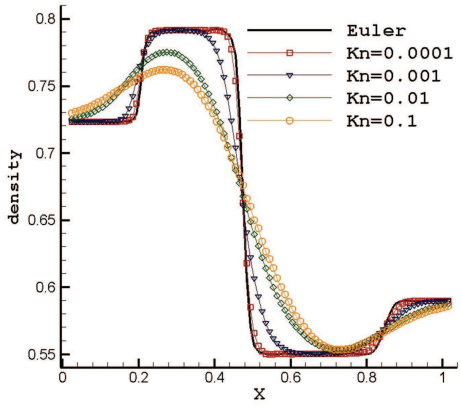

Figure 3: Application of different Knudsen numbers.

flow profiles converge into that solved in the Euler limit as Knudsen number decreases. The effect of rarefaction on the shock tube flow is seen for $Kn=0.1, 0.01$, and 0.001. For such condition (close to the transitional flow regime), the shock profiles are not as conspicuous as they are for a smaller Knudsen number e.g., $Kn=0.0001$.

5.1.3 Recovery to classical limit

In this example, we fix the initial condition as applied in the first, second and third test cases except for the initial fugacities which are decreased on both sides. We respectively set $z_l=0.01126$ and $z_r=0.006$. This is to show how gases of quantum statistics will recover to classical limit under low fugacity. We can see in Fig. 4 that the profiles of density of the three statistics become closer to each other except for some small deviations as the fugacities are decreased. It is noted that the result of Maxwell-Boltzmann gas lies always between that of Fermi-Dirac gas and Bose-Einstein gas.

5.1.4 Comparison with TVD scheme

In this example, the comparison of the results generated by WENO3 and that by TVD is given. The treatment of discrete velocity space and grid points are the same for the two schemes compared. Here, van Leer limiter is applied in the TVD scheme to generate second order accurate solution. The grid points used are 100 and the initial conditions are set to be the same with those of the first example for Fermion gas. The relaxation time is set to be relatively small ($\tau=0.0001$) so that the physical dissipation will not dominate the results. In Fig. 5, we can observe that the result generated by WENO3 is slightly superior to that of the second-order TVD scheme. We note that the small difference between TVD and WENO3 in this case is due to the existence of physical viscosity in the flow. For Euler solution without physical viscosity, the profiles obtained by WENO3 will be sharper than that by TVD scheme.

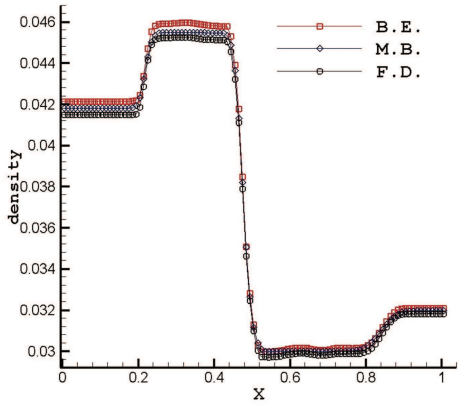

Figure 4: Test on low fugacities (recovery to classical limit).

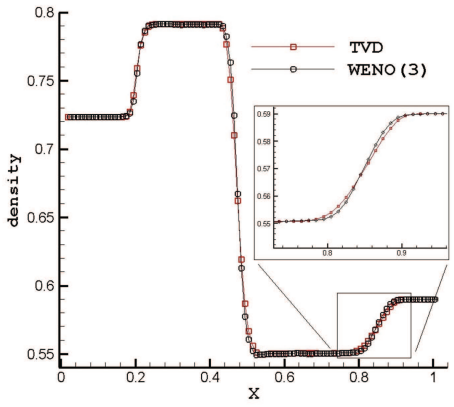

Figure 5: Comparison with TVD scheme on case: $\tau=0.0001$.

5.2 Two-dimensional Riemann problems

Following the works of Lax and Liu, [22] and Schultz-Rinne et al. [31], we selected several configurations to be tested among those of the above-cited papers. In the Riemann problems of two-dimensional gas dynamics, the initial state is in equilibrium and kept constant in each of the four quadrants. See the illustration in Fig. 1. The set up is made so that only one elementary wave, a 1-D shock, $\vec{S}$, a 1-D rarefaction wave, $\vec{R}$, or a 2-D contact discontinuity, J, appears at each interface. To satisfy these constraints, the set initial data must satisfy the Rankine-Hugoniot relations i.e., for a given left an right state (denoted by the indices l and r), we define

$$\Phi_{lr}=\frac{2\sqrt{\gamma}}{\gamma-1}\left(\sqrt{\frac{P_l}{n_l}}-\sqrt{\frac{P_r}{n_r}}\right), \tag{5.1a}$$

$$\Psi_{lr}^2=\frac{(P_l-P_r)(n_l-n_r)}{n_l n_r}, \qquad \Psi_{lr}>0, \tag{5.1b}$$

$$\Pi_{lr}=\left(\frac{P_l}{P_r}+\frac{(\gamma-1)}{(\gamma+1)}\right)/\left(1+\frac{(\gamma-1)P_l}{(\gamma+1)P_r}\right). \tag{5.1c}$$

For cases that include rarefaction waves or shocks, these equations are respectively applied,

$$n_l/n_r=(P_l/P_r)^{1/\gamma} \quad \text{or} \quad n_l/n_r=\Pi_{lr}. \tag{5.2}$$

In this two-dimensional formulation, $\gamma=2$ is chosen. All cases are tested with both 200×200 and 400×400 spatial grid points with $v_\sigma=v_1,v_2,\cdots,v_{20}$ and $v_\delta=v_1,v_2,\cdots,v_{20}$. As an addition to the application of WENO3, results generated with TVD will also be shown for comparison purpose. Van Leer's limiter is applied to generate a second order accuracy in

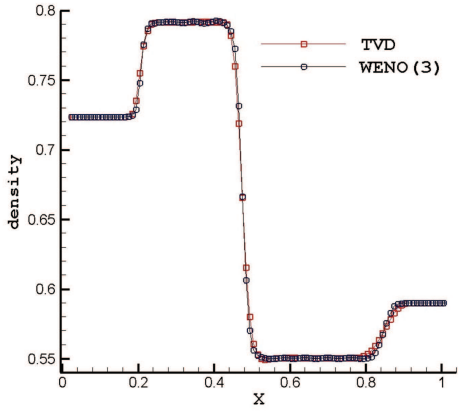

Figure 6: Comparison with TVD scheme on Euler limit.

x and y for the case of TVD. In the case of Euler solutions, it is assumed that $f_{\sigma,\delta}=f^{eq}_{\sigma,\delta}$ so that the collision term automatically vanishes, thus yields an Euler limit solution. We will also apply various values of constant relaxation times to achieve Navier-Stokes solution.

5.2.1 Tests on the three statistics with the setup of config. 13

In this subsection, we test the class of 2-D Riemann's problem with the following initial set up for configuration 13,

$$J_{21},\overleftarrow{S}_{32},J_{34},\overrightarrow{S}_{41}, \qquad P_1=P_2>P_3=P_4, \tag{5.3a}$$

$$u_{x1}=u_{x2}=u_{x3}=u_{x4}, \tag{5.3b}$$

$$u_{y4}-u_{y1}=\Psi_{41}, \qquad u_{y3}-u_{y2}=\Psi_{32}. \tag{5.3c}$$

The initial conditions set in the four quadrants are

$$\begin{matrix} z_2=0.4253 & u_{y2}=0.3 \\ u_{x2}=0 & T_2=1.1494 \end{matrix}\ ', \qquad \begin{matrix} z_1=0.142 & u_{y1}=-0.3 \\ u_{x1}=0 & T_1=2.0782 \end{matrix}\ ', \tag{5.4a}$$

$$\begin{matrix} z_3=0.4448 & u_{y3}=0.697 \\ u_{x3}=0 & T_3=0.7083 \end{matrix}\ ', \qquad \begin{matrix} z_4=0.151 & u_{y4}=0.26254 \\ u_{x4}=0 & T_4=1.273 \end{matrix}\ . \tag{5.4b}$$

We shall expect the slip lines J_{21} and J_{34} to separate the solution into a left and right section while the shocks $\overleftarrow{S}_{32}$ and $\overrightarrow{S}_{41}$ to propagate with their respective set velocities. The results are generated with 200×200 grid points using WENO3 scheme in two space dimensions. All figures are displayed with 30 contour lines. Here, a constant relaxation time $\tau=0.0001$ is applied for the cases of all the three statistics with CFL number set to be 0.1. In Figs. 7 to 12, we can see the plots of density of all the three statistics along with pressure plot for the case of Fermi gas and fugacity plots for the case of the other two

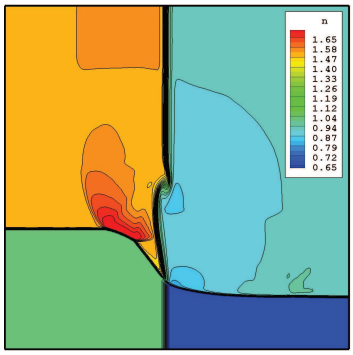

Figure 7: Density contour of Configuration 13: Maxwell-Boltzmann with WENO3 scheme. $\tau = 0.0001$.

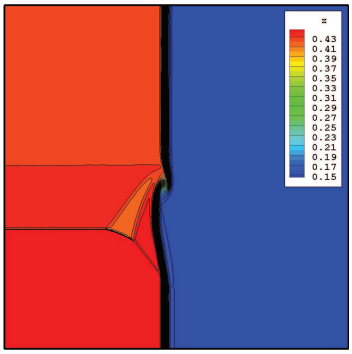

Figure 8: Fugacity contour of Configuration 13: Maxwell-Boltzmann with WENO3 scheme. $\tau = 0.0001$.

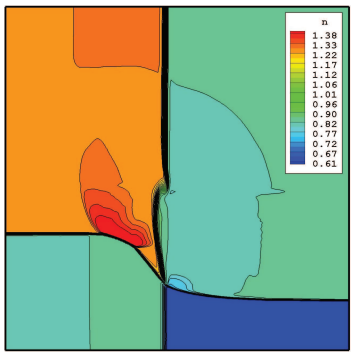

Figure 9: Density contour of Configuration 13: Fermi-Dirac with WENO3 scheme. $\tau = 0.0001$.

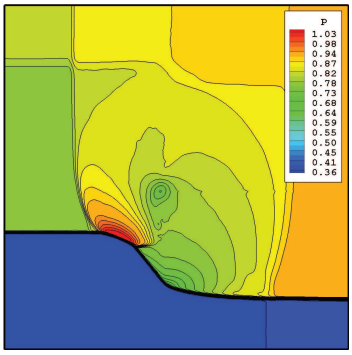

Figure 10: Pressure contour of Configuration 13: Fermi-Dirac with WENO3 scheme. $\tau = 0.0001$.

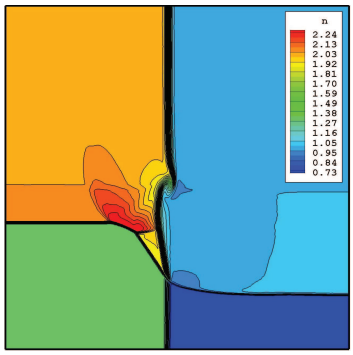

Figure 11: Density contour of Configuration 13: Bose-Einstein with WENO3 scheme. $\tau = 0.0001$.

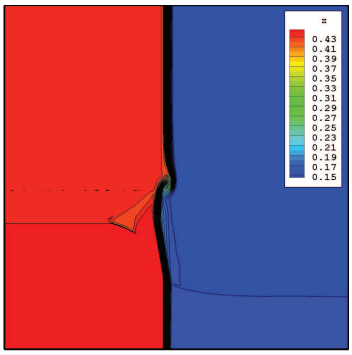

Figure 12: Fugacity contour of Configuration 13: Bose-Einstein with WENO3 scheme. $\tau = 0.0001$.

statistics. The color legends are given with which we can observe the values of densities, fugacities and pressure. The top and bottom peaks of Maxwell-Boltzmann density values, as one can see from the figures, are higher than Fermi-Dirac gas and is lower than Bose-Einstein gas. Aside from value differences between the three statistics, from the density contours in these figures it can be seen that the roll-ups of slip lines in Bose-Einstein gas make the biggest vortex followed respectively by Maxwell-Boltzmann and Fermi-Dirac gases. The difference could be attributed to the different particle effects between these three statistics which generates different viscosities. Additionally, one can refer to [32, 41] to see the effect of different particle statistics. The shown results are in a good agreement with those discussed in the work of Lax [22]. However, the additional application of relaxation time $\tau=0.0001$ and less usage of grid points (200×200) result in more smeared profiles of densities. In addition to the previous works, we are able to provide the plots of fugacity contours which in this case displayed for Maxwell-Boltzmann and Bose-Einstein gases.

5.2.2 Application of various constant relaxation times

We now test the algorithm with the application of varying constant relaxation times. Although an application of constant relaxation times is more of a numerical test rather than physical, we can still show that, based on the relation $\tau=\eta/P$ that this present algorithm can yield an analysis that includes the effect of physical viscosity. In this test, 200×200 grid points in x and y directions along with WENO3 scheme are used in the computation. 20×20 points of abscissas along with the Gauss-Hermite quadrature rule are applied. The Configuration 17 is simulated with the following initial setup: *Configuration 17*.

$$J_{21},\overleftarrow{S_{32}},J_{34},\overrightarrow{R_{41}}, \qquad P_1=P_2>P_3=P_4, \tag{5.5a}$$

$$u_{x1}=u_{x2}=u_{x3}=u_{x4}, \tag{5.5b}$$

$$u_{y4}-u_{y1}=\Phi_{41}, \qquad u_{y3}-u_{y2}=\Psi_{32}, \tag{5.5c}$$

and

$$\begin{matrix} z_2=0.37 & u_{y2}=-0.3 \\ u_{x2}=0 & T_2=1.25 \end{matrix}, \qquad \begin{matrix} z_1=0.14 & u_{y1}=-0.4 \\ u_{x1}=0.1 & T_1=2.08 \end{matrix}, \tag{5.6a}$$

$$\begin{matrix} z_3=0.38 & u_{y3}=0.12 \\ u_{x3}=0 & T_3=0.77 \end{matrix}, \qquad \begin{matrix} z_4=0.14 & u_{y4}=-0.98 \\ u_{x4}=0 & T_4=1.31 \end{matrix}. \tag{5.6b}$$

In this configuration, shock, slip discontinuity and rarefaction fan are expected to be seen propagating from interfaces of the four quadrants. A shock shall be seen propagating through quadrants 3 and 2, rarefaction fan through quadrants 4 and 1 and slip discontinuities through quadrants 2 and 1 and through quadrants 4 and 1. In Figs. 13 and 14 we can see the density plot of Configuration 17 for Maxwell-Boltzmann gases with the application of $\tau=0.0005$ and $\tau=0.01$. In these figures, we see more of the effect of dissipation as the value of τ increases. For example, at $\tau=0.01$ we can see how the flow profiles

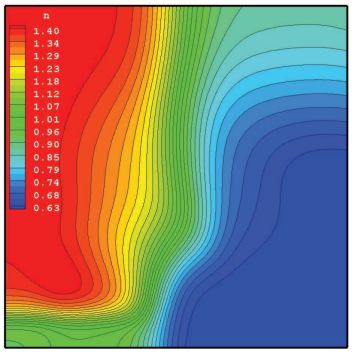

Figure 13: $\tau = 0.01$, density contour. Application of different values of Relaxation times on Maxwell-Boltzmann gas (Config. 17).

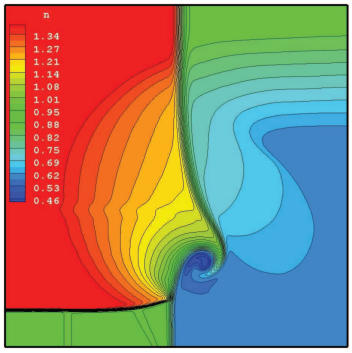

Figure 14: $\tau = 0.0005$, density contour. Application of different values of Relaxation times on Maxwell-Boltzmann gas (Config. 17).

become very smeared compared to the results with smaller relaxation time values. In the application of BGK source terms in these range tested in this paper, we did not experience stiffness problems due to source terms. However, we are aware that such problem can possibly appear under different circumstances. Interested reader could refer to the work of Shi [18–20] which describes a method to tackle stiffness problem.

5.3 Mesh refinement and comparison to TVD scheme

In this subsection, we present the results using refined grid mesh of 400×400 points using (i) WENO3 scheme and (ii) TVD scheme for the purpose of comparison. Here, the usage of TVD scheme instead of WENO3 scheme is the only difference between the two cases, while other initial attributes are applied similarly. Note that all the previous two dimensional examples shown are generated using 200×200 grid points. Thus this example also gives us an illustration of high mesh points convergence. The problem is initially set for Bose gas with $\tau = 0.0001$. The initial condition of Bose gas is adjusted to

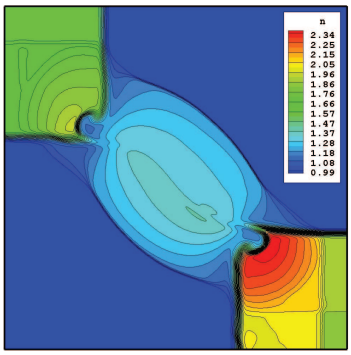

Figure 15: Density contour using TVD spatial discretization on configuration 5. $\tau = 0.0001$.

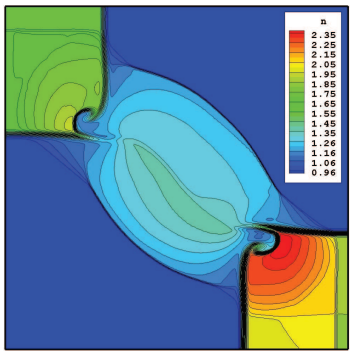

Figure 16: Density contour using WENO3 spatial discretization on configuration 5. $\tau = 0.0001$.

that of configuration 5, i.e., *Configuration 5*.

$$J_{21}, J_{32}, J_{34}, J_{41}, \qquad P_1 = P_2 = P_3 = P_4, \tag{5.7a}$$

$$u_{x1} = u_{x2} < u_{x3} = u_{x4}, \qquad u_{y1} = u_{y4} < u_{y3} = u_{y2}, \tag{5.7b}$$

and

$$\begin{array}{llll} z_2 = 0.4253 & u_{y2} = 0.5 & z_1 = 0.142 & u_{y1} = -0.5 \\ u_{x2} = -0.75 & T_2 = 1.1494 \ , & u_{x1} = -0.75 & T_1 = 2.078 \ , \end{array} \tag{5.8a}$$

$$\begin{array}{llll} z_3 = 0.142 & u_{y3} = 0.5 & z_4 = 0.6635 & u_{y4} = -0.5 \\ u_{x3} = 0.75 & T_3 = 2.078 \ , & u_{x4} = 0.75 & T_4 = 0.8768 \ . \end{array} \tag{5.8b}$$

Here, only slip discontinuities are expected to propagate from each interfaces. The CFL numbers are set to be 0.1. The quadrature rule used is Gauss-Hermite rule with 20 abscissas both in v_x and v_y directions. In Figs. 15 and 16, due to the difference in the order of accuracy, we can see the comparison in which WENO3 outperform TVD in terms of flow profiles sharpness when considered under the same numerical treatment. Note that the purpose of the authors is not to subordinate TVD in comparison to WENO3 since these two methods are of two different order of accuracy. Although the kind of gas used in this example is Bose gas, the results are comparable to the earlier work of Lax [22] (classical gas) in terms of the expected form of flows. Note that the application of constant relaxation time, although small, contribute to a more diffusive form of flows.

6 Concluding remarks

In this work, an accurate algorithm for solving the initial value problems of the semiclassical Boltzmann-BGK transport equation using the discrete ordinate method and fifth-order accurate WENO3 scheme is presented. The former is used to remove the dependency of the distribution functions on molecular velocity while the latter is used to solve a set of discretized conservation laws with source terms. The results see the method applied to one-dimensional shock tube problems and two-dimensional Riemann problems for dilute gas flows of arbitrary particle statistics. Different aspects of the present algorithm are tested including ranges of constant relaxation time values, various Knudsen numbers and physical relaxation times. These computational examples serve the purpose of testing the robustness of the present method. The demonstration of how Fermi and Bose gas will behave in the low fugacities is also given and explained. When the flow Knudsen number is small in the continuum regime, all the expected flow profiles comprising shock, rarefaction wave and contact discontinuities in both one- and two-dimensional examples can be seen with considerably good details and are in good agreement with available results. Moreover, with this algorithm, we are able to present the fugacity plots even for gases within Maxwell-Boltzmann statistics. The feasibility of this algorithm and its capability in describing the gas flows of arbitrary particle statistics in

various flow regimes have been illustrated without much major constraints. The present work emphasizes on building the unified and parallel framework for treating semiclassical rarefied gas dynamics and examinating the flow physics of the three different gas particle statistics under the same hydrodynamic flow conditions. Specific application to different individual carrier in specific physical problem can be individually investigated such as electrons transport [7, 26] or phonons [15] or the electron-phonon transport [29] and will be the subject of future endeavor. Direct extension to three-dimensional cases and more complex geometries in general coordinates are straightforward and will be reported elsewhere.

Acknowledgments

The authors thank Dr. J. C. Huang and Dr. Y. H. Shi for many fruitful discussions. The authors would also like to acknowledge the National Center for High-Performance Computing in providing resources under the national project Knowledge Innovation National Grid in Taiwan. This work is done under the auspices of National Science Council, TAIWAN through grants NSC-99-2922-I-606-002 and CQSE subproject No. 5 99R-80873. Z. H. Li and H. X. Zhang would like to thank the support by project No. 599R-80873 and by National Nature Science Foundation of China under grant No. 91016027.

References

[1] M. Abramowitz and I. A. Stegun. Handbook of Mathematical Functions with Formulas, Graphs, and Mathematical Tables. Dover, New York, ninth dover printing, tenth gpo printing edition, 1964.

[2] M. G. Ancona and G. J. Iafrate. Quantum correction to the equation of state of an electron gas in a semiconductor. Phys. Rev. B, 39(13):9536–9540, May 1989.

[3] M. G. Ancona and H. F. Tiersten. Macroscopic physics of the silicon inversion layer. Phys. Rev. B, 35(15):7959–7965, May 1987.

[4] P. L. Bhatnagar, E. P. Gross, and M. Krook. A model for collision processes in gases. i. small amplitude processes in charged and neutral one-component systems. Phys. Rev., 94(3):511–525, May 1954.

[5] J. A. Carrillo, I. M. Gamba, A. Majorana, and C.-W. Shu. A weno-solver for the 1d non-stationary boltzmannVpoisson system for semiconductor devices. Journal of Computational Electronics, 1:365–370, 2002. 10.1023/A:1020751624960.

[6] J. A. Carrillo, I. M. Gamba, A. Majorana, and C.-W. Shu. A direct solver for 2d non-stationary boltzmann-poisson systems for semiconductor devices: A mesfet simulation by weno-boltzmann schemes. Journal of Computational Electronics, 2:375–380, 2003. 10.1023/B:JCEL.0000011455.74817.35.

[7] J. A. Carrillo, I. M. Gamba, A. Majorana, and C.-W. Shu. A weno-solver for the transients of boltzmann-poisson system for semiconductor devices: performance and comparisons with monte carlo methods. Journal of Computational Physics, 184(2):498 – 525, 2003.

[8] S. Chapman and T. G. Cowling. The mathematical theory of non-uniform gases: an account of the kinetic theory of viscosity, thermal conduction, and diffusion in gases. Cambridge University Press, 1970.
[9] G. Chen. Nanoscale Energy Transport and Conversion: A Parallel Treatment of Electrons, Molecules, Phonons, and Photons (Mit-Pappalardo Series in Mechanical Engineering). Oxford University Press, USA, Mar. 2005.
[10] X. G. Deng and H. X. Zhang. Developing high-order weighted compact nonlinear schemes. Journal of Computational Physics, 165:24–44, 2000.
[11] E. Fatemi and F. Odeh. Upwind finite difference solution of boltzmann equation applied to electron transport in semiconductor devices. Journal of Computational Physics, 108(2):209 – 217, 1993.
[12] C. L. Gardner. The quantum hydrodynamic model for semiconductor devices. SIAM J. Appl. Math., 54(2):409–427, 1994.
[13] A. Harten. High resolution schemes for hyperbolic conservation laws. Journal of Computational Physics, 49(3):357 – 393, 1983.
[14] A. Harten and P. D. Lax. On a class of high resolution total-variation-stable finite-difference schemes. SIAM Journal on Numerical Analysis, 21(1):pp. 1–23, 1984.
[15] T.-Y. Hsieh and J.-Y. Yang. Thermal conductivity modeling of circular-wire nanocomposites. Journal of Applied Physics, 108:044306, 2010.
[16] A. B. Huang and D. P. Giddens. The Discrete Ordinate Method for the Linearized Boundary Value Problems in Kinetic Theory of Gases. In C. L. Brundin, editor, Rarefied Gas Dynamics, Volume 1, pages 481–+, 1967.
[17] G.-S. Jiang, D. Levy, C.-T. Lin, S. Osher, and E. Tadmor. High-resolution nonoscillatory central schemes with nonstaggered grids for hyperbolic conservation laws. SIAM Journal on Numerical Analysis, 35(6):pp. 2147–2168, 1998.
[18] S. Jin. Runge-kutta methods for hyperbolic conservation laws with stiff relaxation terms. J. Comput. Phys, 122:51–67, 1995.
[19] S. Jin and C. D. Levermore. Numerical schemes for hyperbolic conservation laws with stiff relaxation terms. J. Comput. Phys, 126:449–467, 1996.
[20] S. Jin and Z. P. Xin. The relaxation schemes for systems of conservation laws in arbitrary space dimensions. Communications on Pure and Applied Mathematics, 48:235, 2006.
[21] L. P. Kadanoff and G. Baym. Quantum Statistical Mechanics. Benjamin, New York, 1962.
[22] P. D. Lax and X. D. Liu. Solution of two dimensional riemann problem of gas dynamics by positive schemes. SIAM J. Sci. Comput, 19:319–340, 1995.
[23] Z.-H. Li and H.-X. Zhang. Numerical investigation from rarefied flow to continuum by solving the boltzmann model equation. Intern. J. Numer. Fluids, 42:361–382, 2003.
[24] Z.-H. Li and H.-X. Zhang. Study on gas kinetic unified algorithm for flows from rarefied transition to continuum. Journal of Computational Physics, 193:708–738, 2004.
[25] M. Lundstrom. Fundamentals of Carrier Transport. Cambridge University Press, 2nd edition, 2000.
[26] A. Majorana and R. M. Pidatella. A finite difference scheme solving the boltzmann-poisson system for semiconductor devices: Volume 174, number 2 (2001), pages 649-668. Journal of Computational Physics, 177(2):450 – 450, 2002.
[27] P. A. Markowich, C. A. Ringhofer, and C. Schmeiser. Semiconductor Equations. Springer, 1 edition, 2002.
[28] T. Nikuni and A. Griffin. Hydrodynamic damping in trapped bose gases. Journal of Low Temperature Physics, 111:793–814, 1998.

[29] A. Pattamatta and C. K. Madnia. Modeling electron-phonon nonequilibrium in gold films using boltzmann transport model. Journal of Heat Transfer, 131:082401–1, 2009.
[30] S. Scaldaferri, G. Curatola, and G. Iannaccone. Direct solution of the boltzmann transport equation and poisson schrodinger equation for nanoscale mosfets. IEEE Transaction on Electron Devices, 54:2901, 2007.
[31] C. W. Schultz-Rinne, J. P. Collins, and H. M. Glaz. Numerical solution of the riemann problem for two-dimensional gas dynamics. SIAM J. Sci. Comput., 14(6):1394–1414, 1993.
[32] Y. H. Shi and J. Y. Yang. A gas kinetic bgk scheme for semiclassical boltzmann hydrodynamic transport. Journal of Computational Physics, 227(22):9389 – 9407, 2008.
[33] B. Shizgal. A gaussian quadrature procedure for use in the solution of the boltzmann equation and related problems. Journal of Computational Physics, 41(2):309 – 328, 1981.
[34] E. A. Uehling and G. E. Uhlenbeck. Transport phenomena in einstein-bose and fermi-dirac gases. i. Phys. Rev., 43(7):552–561, Apr 1933.
[35] B. van Leer. Towards the ultimate conservative difference scheme. v. a second-order sequel to godunov's method. Journal of Computational Physics, 32(1):101 – 136, 1979.
[36] E. Wigner. On the quantum correction for thermodynamic equilibrium. Phys. Rev., 40(5):749–759, Jun 1932.
[37] D. L. Woolard, H. Tian, M. A. Littlejohn, K. W. Kim, R. J. Trew, M. K. Ieong, and T. W. Tang. Construction of higher-moment terms in the hydrodynamic electron transport model. Journal of Applied Physics, 74(10):6197 –6207, nov 1993.
[38] Z. Xu and C.-W. Shu. Anti-diffusive flux corrections for high order finite difference weno schemes. Journal of Computational Physics, 205(2):458 – 485, 2005.
[39] J. Y. Yang, T. Y. Hsieh, and Y. H. Shi. Kinetic flux vector splitting schemes for ideal quantum gas dynamics. SIAM J. Sci. Comput., 29(1):221–244, 2007.
[40] J. Y. Yang and J. C. Huang. Rarefied flow computations using nonlinear model boltzmann equations. Journal of Computational Physics, 120(2):323 – 339, 1995.
[41] J. Y. Yang and Y. H. Shi. A kinetic beam scheme for ideal quantum gas dynamics. Proceedings of the Royal Society A: Mathematical, Physical and Engineering Science, 462(2069):1553–1572, 2006.
[42] H.-X. Zhang. Non-oscillatory and non-free-parameter dissipation difference scheme. Acta Aerodynamica Sinica, 9(6):143–165, 1988.